# Excess Wings in Broadband Dielectric Spectroscopy

C. Candelaresi[1,2] and R. Hilfer[3]

[1]Division of Mathematics, University of Dundee
Dundee, DD1 4HN, United Kingdom
[2]NORDITA, AlbaNova University Center
Roslagstullsbacken 23, 10691 Stockholm, Sweden
[3]Institut für Computer Physik, Universität Stuttgart
Pfaffenwaldring 27, 70569 Stuttgart, Germany

originally published in: AIP Conference Proceedings, Vol. 1637, pages 1283-1290
originally submitted: 2014

**Abstract**

Analysis of excess wings in broadband dielectric spectroscopy data of glass forming materials provides evidence for anomalous time evolutions and fractional semigroups. Solutions of fractional evolution equations in frequency space are used to fit dielectric spectroscopy data of glass forming materials with a range between 4 and 10 decades in frequency. It is shown that with only three parameters (two relaxation times plus one exponent) excellent fits can be obtained for 5-methyl-2-hexanol and for methyl-m-toluate over up to 7 decades. The traditional Havriliak-Negami fit with three parameters (two exponents and one relaxation time) fits only 4-5 decades. Using a second exponent, as in Havriliak-Negami fits, the $\alpha$-peak and the excess wing can be modeled perfectly with our theory for up to 10 decades for all materials at all temperatures considered here. Traditionally this can only be accomplished by combining two Havriliak-Negami functions with 7 parameters. The temperature dependent relaxation times are fitted with the Vogel-Tammann-Fulcher relation which provides the corresponding Vogel-Fulcher temperatures. The relaxation times turn out to obey almost perfectly the Vogel-Tammann-Fulcher law. Computable expressions of time dependent relaxation functions are also reported.

Contents



*keywords*: time evolution, anomalous dynamics, fractional derivatives, glass transition, excess wing, dielectric spectroscopy
PACS: 77.22.Gm,64.70.Q-,77.22.Ch,64.70.pj,77.84.Jd,02.60.Nm

*[page 1283, §1]*

## 1. Introduction

*[1283.1.1]* Many physical properties of glass forming liquids (e.g. their viscosity) vary dramatically (often over 15 or more decades) within a narrow temperature interval around the glass transition [1]. *[1283.1.2]* The change of physical properties during the glass transition has not yet been fully understood and remains a subject of intense investigations [2, 3, 4, 5, 6, 7, 8, 9, 10, 11, 12].

*[1283.2.1]* In this work we study the glass transition by investigating the dielectric susceptibility. *[1283.2.2]* The dielectric susceptibility quantifies the response of permanent and induced dipoles to an applied frequency dependent electric field. *[1283.2.3]* The dielectric loss (resp. imaginary part of the complex dielectric susceptibility) typically shows a temperature dependent maximum, the $\alpha$-peak, at low frequencies. *[1283.2.4]* It is followed at higher frequencies by a so-called excess wing [13]. *[1283.2.5]* This excess wing has not yet been understood nor has it been described by any model with less than 4 fit parameters [13]. *[1283.2.6]* Existing theories, such as the mode coupling theory (see [14, 15] and references therein), do not allow to fit the excess wing. *[1283.2.7]* Traditional phenomenological fits of the excess wing employ a superposition of two Havriliak-Negami functions [16, 5, 13], and they need 7 fit parameters to fit a range of 10 decades.

*[1283.3.1]* The aim of this work is to provide analytical expressions for excess wings with only three and four parameters. *[1283.3.2]* The formulae are obtained from the previously introduced method of fractional time evolution [17, 18, 19], and applied to experimental data exhibiting a clear excess wing over a frequency range as broad as possible. *[1283.3.3]* The fit functions need only three parameters (one exponent and two relaxation times in model A) or four parameters (two exponents and two relaxation times for model B). *[1283.3.4]* This is a significant improvement compared to six parameters for the superposition of the Havriliak-Negami and Cole-Cole expression presently used [19, 20]. *[1283.3.5]* We study the glass forming materials 5-methyl-2-hexanol [6], glycerol [8] and methyl-m-toluate [12].

## 2. Classical relaxation models

*[1283.4.1]* The Debye relaxation model describes the electric relaxation of dipoles after switching an applied electric field [21]. *[1283.4.2]* The normalized relaxation function $f(t)$, which corresponds to the polarization, obeys the Debye law

$$\left(\tau\frac{\mathrm{d}}{\mathrm{d}t}+1\right)f(t)=0, \tag{1}$$

*[page 1284, §0]* with the relaxation time $\tau$ and initial condition $f(0)=1$. *[1284.0.1]* The response function, i.e. the dynamical dielectric susceptibility, $\chi$ is related to the relaxation function via [17]

$$\chi(t)=-\frac{\mathrm{d}}{\mathrm{d}t}f(t). \tag{2}$$

| | functional form $\hat{\chi}(u)$ | number of parameters |
|---|---|---|
| Cole-Cole | $1/(1+(u\tau)^{\alpha})$ | 2 |
| Cole-Davidson | $1/(1+u\tau)^{\alpha}$ | 2 |
| Havriliak-Negami | $1/(1+(u\tau)^{\alpha})^{\gamma}$ | 3 |

TABLE 1. List of traditional fit functions for dielectric spectroscopy data of glass forming materials.

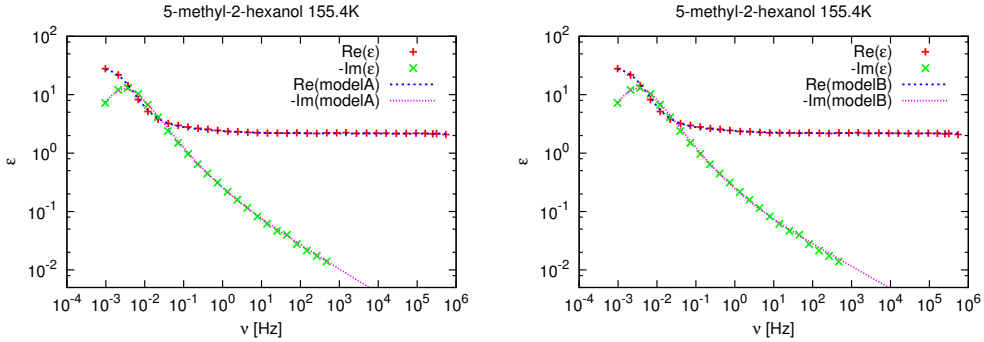


FIGURE 1. Simultaneous fits of real and imaginary part with model A (left figure) and model B (right figure) for 5-methyl-2-hexanol at 155.4 K. Both models show an excellent fitting capability. The data are from [6].

*[1284.0.2]* In the following discussions we focus on Laplace transformed quantities. *[1284.0.3]* We use the Laplace transformation of $f(t)$

$$\mathscr{L}\{f(t)\}(u) = \int_0^\infty e^{-ut} f(t)\ \mathrm{d}t, \tag{3}$$

where $u = i\nu$ and $\nu$ is the frequency. *[1284.0.4]* Rewriting equation (2) in frequency space and using $f(0) = 1$ leads to

$$\hat{\chi}(u) = \mathscr{L}\{\chi(t)\}(u) = 1 - u\mathscr{L}\{f(t)\}(u) = \frac{1}{1+u\tau}, \tag{4}$$

the well known Debye susceptibility. *[1284.0.5]* In experiments one measures not the normalized quantity $\hat{\chi}(u)$, but instead

$$\varepsilon(u) = (\varepsilon_0 - \varepsilon_\infty)\hat{\chi}(u) + \varepsilon_\infty, \tag{5}$$

where $\varepsilon_0$ and $\varepsilon_\infty$ are the dynamical susceptibilities at low, respectively high frequencies.

*[1284.1.1]* The Debye model is not able to describe the experimental data well, because experimental relaxation peaks are broader and asymmetric. *[1284.1.2]* For this reason other fitting functions were proposed such as the Cole-Cole [22], Cole-Davidson [23] and Havriliak-Negami [16] expressions. *[1284.1.3]* Their normalized forms have typically 2 or 3 parameters (see table 1) and they were introduced purely phenomenologically to fit the data. *[1284.1.4]* This can be considered as a drawback. *[1284.1.5]* These functions with three parameters are able to fit the data over a range of at most 5 decades (Havriliak-Negami). *[1284.1.6]* To fit a broader frequency range several functions are commonly added. *[1284.1.7]* A combination of one Havriliak-Negami expression plus one Cole-Cole form results in 6 fit parameters.

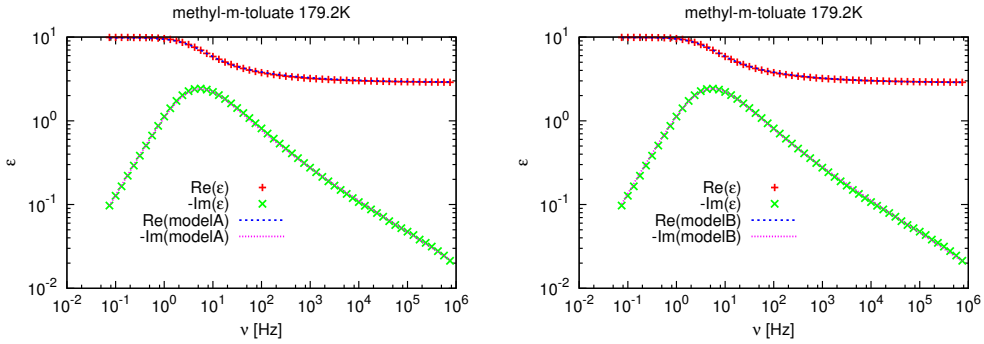


FIGURE 2. Simultaneous fits of real and imaginary part with model A (left figure) and model B (right figure) for methyl-m-toluate at 179.2 K. Model A can fit the data over the whole spectral range of 7 decades, which is more than with Havriliak-Negami which uses the same number of fit parameters. With this data we obtain the broadest fit with model A. The data are from [12].

## 3. Fractional relaxation models

*[1284.2.1]* In this work we use a generalized form of the Debye relaxation model from eq. (1). *[1284.2.2]* It is based on the theory of fractional time evolutions for macroscopic states of many body systems first proposed in equation (5.5) in [24] and subsequently elaborated in [25, 26, 27, 28, 29, 30, 17, 31, 32, 33, 34]. *[1284.2.3]* As discussed in [30, 17] composite fractional time evolutions are expected near the glass transition. *[1284.2.4]* Such time evolutions give rise to generalized Debye laws of the form of model A:

$$(\tau_1 \mathrm{D} + \tau_2^\alpha \mathrm{D}^\alpha + 1)\, f(t) = 0 \tag{6}$$

or model B:

$$(\tau_1 \mathrm{D} + \tau_1^{\alpha_1} \mathrm{D}^{\alpha_1} + \tau_2^{\alpha_2} \mathrm{D}^{\alpha_2} + 1)\, f(t) = 0, \tag{7}$$

where the parameters obey $0 < \alpha, \alpha_1, \alpha_2 < 1$, $\alpha_1 > \alpha_2$ and the relaxation times $\tau_1, \tau_2 > 0$ are positive. *[1284.2.5]* Here the symbols $\tau_1 \mathrm{D} + \tau_2^\alpha \mathrm{D}^\alpha$, respectively $\tau_1 \mathrm{D} + \tau_1^{\alpha_1} \mathrm{D}^{\alpha_1} + \tau_2^{\alpha_2} \mathrm{D}^{\alpha_2}$ are the infinitesimal generators of composite fractional semigroups *[page 1285, §0]* with $\mathrm{D}^\alpha$ being a generalized fractional Riemann-Liouville derivative of order $\alpha$ and almost any type [29, 35]. *[1285.0.1]* If $\mathrm{D}^\nu$ represents a classical fractional Riemann-Liouville derivative of order $\nu$ then its definition reads (with $\nu \in \mathbb{R}^+$)

$$\mathrm{D}^\nu f(t) = \mathrm{D}^{\lceil \nu \rceil} \mathrm{I}^\mu f(t) \tag{8}$$

$$= \frac{1}{\Gamma(\mu)} \mathrm{D}^{\lceil \nu \rceil} \int_0^t (t-\xi)^{\mu-1} f(\xi)\, \mathrm{d}\xi, \tag{9}$$

$$\mu + \nu = \lceil \nu \rceil, \quad t > 0,$$

where $\lceil \nu \rceil$ is the smallest integer greater or equal $\nu$, $\Gamma$ the gamma function and $\mathrm{D}^{\lceil \nu \rceil} = \mathrm{d}^{\lceil \nu \rceil} / \mathrm{d}t^{\lceil \nu \rceil}$.

*[1285.1.1]* The Laplace transform of the fractional Riemann-Liouville derivative is [36]

$$\mathscr{L}\{\mathrm{D}^\nu f(t)\}(u) = u^\nu \mathscr{L}\{f(t)\}(u) - \sum_{k=1}^{\lceil \nu \rceil} u^{k-1}\, \mathrm{D}^{\nu-k} f(t)\big|_{t=0}\,. \tag{10}$$

*[page 1286, §1]* *[1286.1.1]* With these definitions the Laplace transformation of equations (6) and (7) gives with relation (2) the normalized dielectric susceptibilities of model A

$$\hat{\chi}_{\mathrm{A}}(u) = \frac{1 + \tau_2^{\alpha} u^{\alpha}}{\tau_1 u + \tau_2^{\alpha} u^{\alpha} + 1} \tag{11}$$

and model B

$$\hat{\chi}_{\mathrm{B}}(u) = \frac{1 + \tau_1^{\alpha_1} u^{\alpha_1} + \tau_2^{\alpha_2} u^{\alpha_2}}{\tau_1 u + \tau_1^{\alpha_1} u^{\alpha_1} + \tau_2^{\alpha_2} u^{\alpha_2} + 1}. \tag{12}$$

*[1286.1.2]* These results apply also for other types of generalized Riemann-Liouville fractional derivatives introduced in [30, 17].

*[1286.2.1]* The functions from equations (11) and (12) are used to fit the dielectric spectroscopy data of 5-methyl-2-hexanol, glycerol and methyl-m-toluate. *[1286.2.2]* Real and imaginary part are fitted simultaneously with the parameters $\alpha$, $\alpha_1$, $\alpha_2$, $\tau_1$ and $\tau_2$.

*[1286.3.1]* Additionally we fit the temperature dependent relaxation times $\tau_1$ and $\tau_2$ with the Vogel-Tammann-Fulcher function

$$\tau = \tau_0 \exp\left(\frac{D T_{\mathrm{VF}}}{T - T_{\mathrm{VF}}}\right), \tag{13}$$

where $T$ is the absolute temperature, $\tau_0$ a material parameter, $D$ the fragility and $T_{\mathrm{VF}}$ the Vogel-Fulcher temperature. *[1286.3.2]* The fit parameters are $\tau_0$, $D$ and $T_{\mathrm{VF}}$.

## 4. Results

*[1286.4.1]* Model A fits for 5-methyl-2-hexanol are shown in Fig. 1 and for methyl-m-toluate Fig. 2. *[1286.4.2]* Note that in our notation $\varepsilon = \varepsilon' - i\varepsilon''$. *[1286.4.3]* Model A fits the data remarkably well for five, respectively seven orders of magnitude, where both the $\alpha$-peak and the excess wing can be fitted simultaneously with only three parameters. *[1286.4.4]* Model A is better suited than the Havriliak-Negami model which only fits reasonably well for up to four orders of magnitudes for these materials. *[1286.4.5]* This improvement is due to the positive curvature of the function in (11) at frequencies above the $\alpha$-peak. *[1286.4.6]* Sometimes this curvature poses also the main difficulty when fitting with model A. *[1286.4.7]* An example is glycerol as seen in the left part of Fig. 3. *[1286.4.8]* While it is easy to fit closely the the $\alpha$-peak it is more difficult to simultaneously fit the excess wing.

*[1286.5.1]* Model B can fit the data much better than model A, because it contains one more parameter. *[1286.5.2]* Nevertheless, it is remarkable that it can fit a range of up to 10 orders of magnitude with little deviation from the data points. *[1286.5.3]* We believe that this model can be used to fit over some more orders of magnitude, but at this time there is no experimental data available which covers a broader range.

## 5. Temperature dependence of the parameters

*[page 1287, §1]* *[1287.1.1]* Because the data have been fitted at different temperatures we are able to observe the temperature dependence of the fitting parameters. *[1287.1.2]* For $\tau_1$

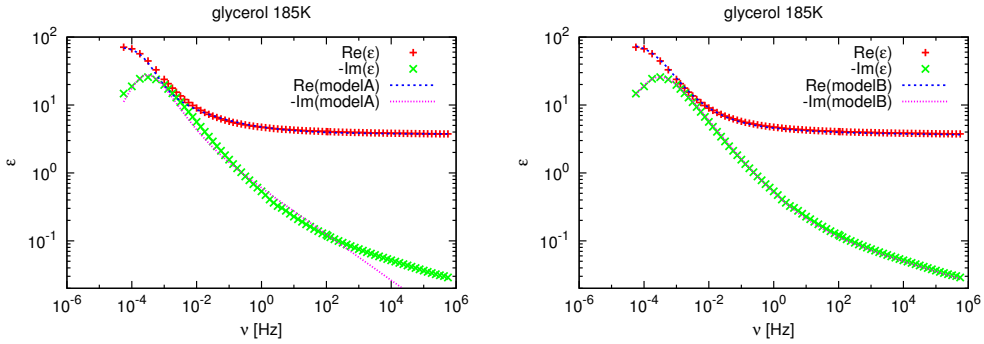


FIGURE 3. Simultaneous fits of real and imaginary part with model A (left figure) and model B (right figure) for glycerol at 185 K. While model A is not able to fit the data well, model B still gives an excellent fit over 10 decades. The data are from [8].

| material | model | $T_{\mathrm{VF1}}$ | $T_{\mathrm{VF2}}$ | $D_1$ | $D_2$ | $\tau_{01}$ | $\tau_{02}$ |
|---|---|---|---|---|---|---|---|
| 5-methyl-2-hexanol | A | 89.2 K | 92.1 K | 25.5 | 22.1 | $3.53 \times 10^{-13}$ s | $7 \times 10^{-14}$ s |
| 5-methyl-2-hexanol | B | 88.3 K | 101.6 K | 26.3 | 15.3 | $5.21 \times 10^{-13}$ s | $5.77 \times 10^{-12}$ s |
| methyl-m-toluate | A | 71.2 K | 71.2 K | 93.2 | 93.2 | $4.35 \times 10^{-28}$ s | $1.54 \times 10^{-28}$ s |
| methyl-m-toluate | B | 67.2 K | 85.6 K | 102.2 | 53.6 | $9.0 \times 10^{-28}$ s | $1.13 \times 10^{-22}$ s |
| glycerol | A | 127.8 K | 131.5 K | 17.1 | 14.9 | $3.7 \times 10^{-14}$ s | $3.23 \times 10^{-14}$ s |
| glycerol | B | 152.7 K | 137.8 K | 6.68 | 11.9 | $2.9 \times 10^{-10}$ s | $2.15 \times 10^{-13}$ s |

TABLE 2. List of the fit parameters $T_{\mathrm{VF}}$, $D$ and $\tau_0$ for various materials.

and $\tau_2$ we perform Vogel-Tammann-Fulcher fits provided by equation (13). *[1287.1.3]* From the fits we obtain the Vogel-Fulcher temperatures $T_{\mathrm{VF1}}$ and $T_{\mathrm{VF2}}$ as well as the fragility parameters $D_1$ and $D_2$ for the relaxation times $\tau_1$ and $\tau_2$ for model A and model B (see Table 2).

*[1287.2.1]* For all fits we see a temperature dependence of the relaxation times $\tau_1$ and $\tau_2$ (Fig. 4 - Fig. 6) that follows the Vogel-Tammann-Fulcher fitting function remarkably well. *[1287.2.2]* The relaxation times also show a clear downward trend as the temperature increases, which confirms that $\tau$, $\tau_1$ and $\tau_2$ are physically meaningful and can be interpreted as relaxation times even tough they appear with a non-integer power in equations (11) and (12).

*[1287.3.1]* The parameters $\alpha$, $\alpha_1$ and $\alpha_2$ also show a temperature dependence. *[1287.3.2]* In the case of 5-methyl-2-hexanol (Fig. 4) there is an increase of $\alpha$ with temperature until a plateau near $\alpha = 1$ is reached. *[1287.3.3]* This effect comes from the decreasing slope of the excess wing with increasing temperature. *[1287.3.4]* In the fitting function of model A this behavior can be achieved by increasing $\alpha$. *[1287.3.5]* For the same material there is an apparent increase of $\alpha_2$ between 154 K (6.49 $\mathrm{K}^{-1}$) and 287 K (3.48 $\mathrm{K}^{-1}$) which has the same origin as the increase in $\alpha$ in model A. *[1287.3.6]* By increasing $\alpha_2$ the excess wing becomes less steep. *[1287.3.7]* The plateau at 190 K (5.26 $\mathrm{K}^{-1}$) and above comes from the fact that the fits at those temperatures are done mainly for the $\alpha$-peak, because the excess wing is not visible.

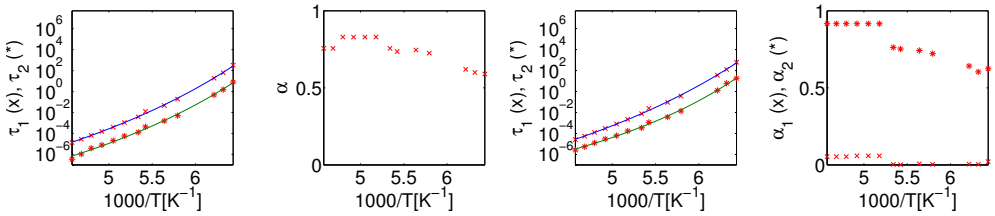


FIGURE 4. Temperature dependence of the fitting parameters $\tau_1$ (crosses), $\tau_2$ (stars) and $\alpha$ for 5-methyl-2-hexanol for model A (left two panels). Temperature dependence of the fitting parameters $\tau_1$ (crosses), $\tau_2$ (stars), $\alpha_1$ (crosses) and $\alpha_2$ (stars) for model B (right two panels). The solid lines are Vogel-Tammann-Fulcher fits (see eq. (13)) whose parameters are listed in Table 2.

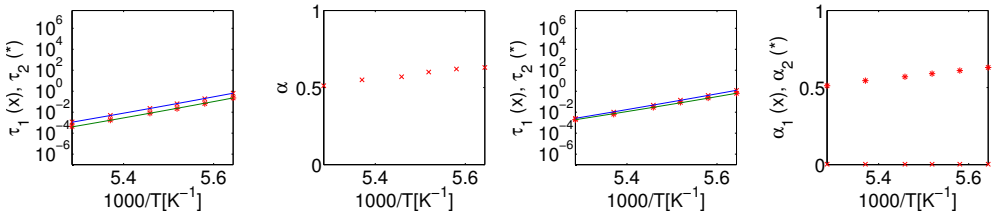


FIGURE 5. Temperature dependence of the fitting parameters $\tau_1$ (crosses), $\tau_2$ (stars) and $\alpha$ for methyl-m-toluate for model A (left two panels). Temperature dependence of the fitting parameters $\tau_1$ (crosses), $\tau_2$ (stars), $\alpha_1$ (crosses) and $\alpha_2$ (stars) for model B (right two panels). The solid lines are Vogel-Tammann-Fulcher fits (see eq. (13)) whose parameters are listed in Table 2.

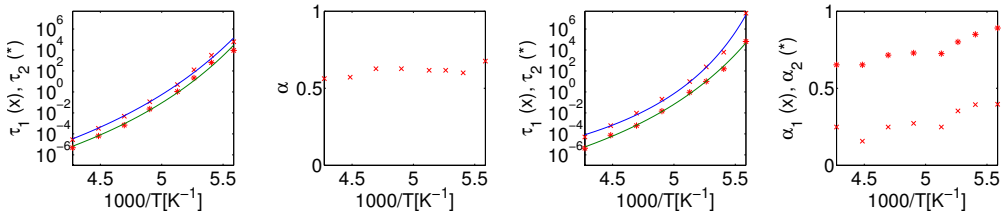


FIGURE 6. Temperature dependence of the fitting parameters $\tau_1$ (crosses), $\tau_2$ (stars) and $\alpha$ for glycerol for model A (left two panels). Temperature dependence of the fitting parameters $\tau_1$ (crosses), $\tau_2$ (stars), $\alpha_1$ (crosses) and $\alpha_2$ (stars) for model B (right two panels). The solid lines are Vogel-Tammann-Fulcher fits (see eq. (13)) whose parameters are listed in Table 2.

*[1287.4.1]* For methyl-m-toluate and glycerol there is also a clear temperature dependence of $\alpha$, $\alpha_1$ and $\alpha_2$ (Fig. 5 and Fig. 6). *[1287.4.2]* The trend is however reversed in comparison to 5-methyl-2-hexanol. *[1287.4.3]* This comes from the increasing slope of the excess wing with increasing temperature. *[1287.4.4]* This behavior can be achieved in the fit functions by decreasing $\alpha$, respectively $\alpha_2$.

## 6. Representation of the solutions as functions of time

*[1287.5.1]* In [20] we obtained the analytical solution of a fractional differential equation of rational order, which we use to analyze our fitting results for model A and model B. *[1287.5.2]* For a general solution of equations (11) and (12) with arbitrary real $\alpha_i$ see [35]. *[1287.5.3]* The restriction to rational $\alpha_i$ is not a drawback, because we can approximate $\alpha_1$ and $\alpha_2$ by a rational value on a grid between 0 and 1. *[1287.5.4]* This number of grid points is chosen to be 20, which keeps computation times reasonably limited as the computing time increases quadratically with the lowest common denominator of $\alpha$ with 1.

*[page 1288, §1]* *[1288.1.1]* The solution for $f(t)$ for model B is a sum of Mittag-Leffler type functions:

$$f(t) = \sum_{j=1}^{N} B_j \sum_{k=0}^{N-1} c_j^{N-k-1} E\left(-k/N, c_j^N; t\right), \tag{14}$$

where $N$ is the smallest number for which both $\alpha_1 N$ and $\alpha_2 N$ are integers. *[1288.1.2]* The coefficients $c_j$ are the zeros of the characteristic polynomial

$$c^N + \tau_1^{\alpha_1} c^{\alpha_1 N} + \tau_2^{\alpha_2} c^{\alpha_2 N} + 1 = 0, \tag{15}$$

the function $E(\nu, a; t)$ is defined as [36]

$$E(\nu, a; t) = t^\nu \sum_{k=0}^{\infty} \frac{(at)^k}{\Gamma(\nu + k + 1)}. \tag{16}$$

*[1288.1.3]* The coefficients $B_j$ are the solutions of the linear system of equations

$$\sum_{k=1}^{N} c_k^i B_k = 0, \qquad 0 \le i \le N - \alpha_1 N - 1 \tag{17}$$

$$\sum_{k=1}^{N} (c_k^i + \tau_1^{\alpha_1} c_k^{i-N+\alpha_1 N}) B_k = 0, \qquad N - \alpha_1 N \le i \le N - \alpha_2 N - 1 \tag{18}$$

$$\sum_{k=1}^{N} (c_k^i + \tau_1^{\alpha_1} c_k^{i-N+\alpha_1 N} + \tau_2^{\alpha_2} c_k^{i-N+\alpha_2 N}) B_k = 0, \qquad N - \alpha_2 N \le i \le N - 2. \tag{19}$$

*[1288.1.4]* This solution is only valid if all the roots $c_j$ of the characteristic polynomial in (15) are distinct, which is checked in the computations. *[1288.1.5]* Because the linear system of equations (17)-(19) is underdetermined we choose one fundamental solution for $\{B_j\}$ and a multiplication factor for $f(t)$ such that $f(0) = 1$.

*[page 1289, §1]* *[1289.1.1]* The analytical solutions are plotted for glycerol at 195 K (Fig. 7). *[1289.1.2]* The fitting values for $\tau$ for model A are $\tau_1 = 4.991$ s and $\tau_2 = 1.089$ s. *[1289.1.3]* Both values lie in the time interval where the relaxation occurs, which confirms the interpretation of these fitting parameters as relaxation times. *[1289.1.4]* For model B the fitted times are $\tau_1 = 9.729$ s and $\tau_2 = 0.92$ s. *[1289.1.5]* So $\tau_2$ marks the onset of the relaxation and $\tau_1$ the end.

*[1289.2.1]* We note that the fractional derivatives appearing in the initial value problem (7) can be generalized to fractional derivatives of arbitrary type $\beta$ introduced in [29] and defined as

$$\mathrm{D}^{\nu,\beta} f(t) = \mathrm{I}^{(1-\beta)(\lceil\nu\rceil-\nu)} \mathrm{D}^{\lceil\nu\rceil} \mathrm{I}^{\beta(\lceil\nu\rceil-\nu)} f(t), \qquad 0 \le \beta \le 1. \tag{20}$$

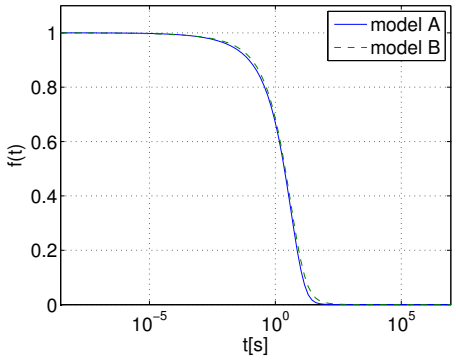


FIGURE 7. The solutions of the fractional initial value problems (6) and (7) with $f(0) = 1$ using the fit parameters for model A and model B for glycerol at 195 K.

*[1289.2.2]* For the case $\beta = 1$ it reduces to the Riemann-Liouville fractional derivative, while for $\beta = 0$ to the Liouville-Caputo-type derivative [33]. *[1289.2.3]* Because

$$\mathrm{D}^{\nu,\beta} E(\mu, a; t) = \mathrm{D}^{\nu,\gamma} E(\mu, a; t), \qquad 0 \leq \beta, \gamma \leq 1, \quad \mu > -1, \quad \nu \geq 0, \tag{21}$$

the solution of our initial value problem does not change by replacing the Riemann-Liouville fractional derivatives with these generalized Riemann-Liouville fractional derivatives of type $\beta$.

## 7. Conclusions

*[1289.3.1]* Two fractional relaxation models (model A and model B) were shown to fit broad band dielectric spectroscopy data for various glass forming materials. *[1289.3.2]* For 5-methyl-2-hexanol and methyl-m-toluate the 3-parameter model A can fit data over a range of 6 and 7 orders of magnitude. *[1289.3.3]* Generally we observed good fits over a range of at least 5 orders of magnitude for model A and 10 orders of magnitude for model B. *[1289.3.4]* Conventional fitting formulae (such as Havriliak-Negami and Cole-Cole) require 6 parameters in contrast to 3 for model A resp. 4 for model B. *[1289.3.5]* In summary, this work has given closed form analytical expressions for excess wings containing only three (or four) parameters, that are derived from the previously introduced method of composite fractional time evolutions [17, 18] and are directly applicable to experiment.

## Acknowledgement

We thank Sebastian Schmiescheck for technical assistance.

## References

[1] P. Lunkenheimer, U. Schneider, R. Brand, and A. Loidl, *Contemporary Physics* **41**, 15 (2000).
[2] P. Lunkenheimer, A. Pimenov, B. Schiener, R. Böhmer, and A. Loidl, *EPL (Europhysics Letters)* **33**, 611 (1996a).
[3] S. Corezzi, S. Capaccioli, G. Gallone, M. Lucchesi, and P. A. Rolla, *Journal of Physics: Condensed Matter* **11**, 10297–10314 (1999).

[4] R. Behrends, K. Fuchs, U. Kaatze, Y. Hayashi, and Y. Feldman, *The Journal of Chemical Physics* **124**, 144512 (2006).

[5] S. Corezzi, M. Beiner, H. Huth, K. Schröter, S. Capaccioli, R. Casalini, D. Fioretto, and E. Donth, *The Journal of Chemical Physics* **117**, 2435–2448 (2002).

[6] O. E. Kalinovskaya, and J. K. Vij, *The Journal of Chemical Physics* **112**, 3262–3266 (2000).

[7] U. Schneider, P. Lunkenheimer, R. Brand, and A. Loidl, *Phys. Rev. E* **59**, 6924–6936 (1999).

[8] P. Lunkenheimer, A. Pimenov, M. Dressel, Y. G. Goncharov, R. Böhmer, and A. Loidl, *Phys. Rev. Lett.* **77**, 318–321 (1996b).

[9] A. Puzenko, Y. Hayashi, Y. Ryabov, I. Balin, Y. Feldman, U. Kaatze, and R. Behrends, *Journal of Physical Chemistry B* **109**, 6031–6035 (2005).

[10] Y. Hayashi, A. Puzenko, I. Balin, Y. Ryabov, and Y. Feldman, *Journal of Physical Chemistry B* **109**, 9174–9177 (2005), ISSN 1520-6106.

[11] T. Hecksher, A. I. Nielsen, O. B. Niels, and D. C. Jeppe, *Nat Phys* **4**, 737 – 741 (2008).

[12] A. I. Nielsen, T. Christensen, B. Jakobsen, K. Niss, N. B. Olsen, R. Richert, and J. C. Dyre, *The Journal of Chemical Physics* **130**, 154508 (2009).

[13] F. Kremer, and A. Schönhals (eds.), *Broadband Dielectric Spectroscopy*, Springer Verlag, Berlin, 2003.

[14] W. Götze, *Condensed Matter Physics* **1**, 873 (1998).

[15] D. R. Reichman, and P. Charbonneau, *Journal of Statistical Mechanics: Theory and Experiment* **2005**, P05013 (2005).

[16] S. Havriliak, and S. Negami, *Journal of Polymer Science Part C: Polymer Symposia* **14**, 99–117 (1966), ISSN 1935-3065.

[17] R. Hilfer, *Chem.Phys.* **284**, 399 (2002a).

[18] R. Hilfer, *Fractals* **11**, 251–257 (2003a).

[19] R. Hilfer, "Applications and Implications of Fractional Dynamics for Dielectric Relaxation", in *Recent Advances in Broadband Dielectric Spectroscopy*, edited by Y. Kalmykov, Springer, Berlin, 2012, p. 123.

[20] S. Candelaresi, *Fraktionale Ansätze in dielektrischer Breitbandspektroskopie*, Master's thesis, Universität Stuttgart (2008).

[21] H. Fröhlich, *Theory of Dielectrics: Dielectric Constant and Dielectric Loss*, Oxford University Press, 1949.

[22] K. S. Cole, and R. H. Cole, *The Journal of Chemical Physics* **9**, 341–351 (1941).

[23] D. W. Davidson, and R. H. Cole, *The Journal of Chemical Physics* **19**, 1484–1490 (1951).

[24] R. Hilfer, *Phys. Rev. E* **48**, 2466 (1993).

[25] R. Hilfer, *Chaos, Solitons & Fractals* **5**, 1475 (1995a).

[26] R. Hilfer, *Fractals* **3**, 549 (1995b).

[27] R. Hilfer, *Physica A* **221**, 89 (1995c).

[28] R. Hilfer, *Applications of Fractional Calculus in Physics*, World Scientific Publ. Co., Singapore, 2000a.

[29] R. Hilfer, "Fractional Time Evolution", in *Applications of Fractional Calculus in Physics*, edited by R. Hilfer, World Scientific, Singapore, 2000b, p. 87.

[30] R. Hilfer, *J.Phys.: Condens. Matter* **14**, 2297 (2002b).

[31] R. Hilfer, "Remarks on Fractional Time", in *Time, Quantum and Information*, edited by L. Castell, and O. Ischebeck, Springer, Berlin, 2003b, p. 235.

[32] R. Hilfer, *Physica A* **329**, 35 (2003c).

[33] R. Hilfer, "Threefold Introduction to Fractional Derivatives", in *Anomalous Transport: Foundations and Applications*, edited by R. Klages, G. Radons, and I. Sokolov, Wiley-VCH, Weinheim, 2008, pp. 17–74.

[34] R. Hilfer, "Foundations of Fractional Dynamics: A Short Account", in *Fractional Dynamics: Recent Advances*, edited by J. Klafter, S. Lim, and R. Metzler, World Scientific, Singapore, 2011, p. 207.

[35] R. Hilfer, Y. Luchko, and Z. Tomovski, *Fractional Calculus and Applied Analysis* **12**, 299 (2009).

[36] K. S. Miller, and B. Ross, *An Introduction to fractional Calculus and fractional Differential Equations*, Wiley-Interscience, 1993.